Hydrostatic compression model for sandy soils

Javier Vallejos

Abstract: Based on elastic considerations, a new four parameter model of the hydrostatic compression curves of sandy soils is presented. Using a unique set of parameters, this model is capable of accurately representing the infinite family of compression curves that result when soil is subjected to stresses below particle breakage. The parameters are readily estimated from two hydrostatic tests conducted at different initial densities during loading and unloading stages. The resulting equations are able to predict the effect of progressive stiffness increase and compressibility reduction that occur as void ratio decreases during both loading and unloading conditions. The same normalized stress scale employed for the hydrostatic compression curves can also be used to describe the steady state line, which leads to a unique framework for representing the stress–void ratio curves of sandy soils. A comprehensive series of simulations on 13 different types of sandy soils in both loose and dense states was performed under a wide range of mean stresses during loading and unloading conditions. The simulations gave very satisfactory agreement with published experimental results.

Key words: hydrostatic compression, constitutive relations, stress–void ratio curves, sandy soils.

Résumé : Sur la base de considérations élastiques, on présente un nouveau modèle à quatre paramètres pour la représentation des courbes de compression hydrostatique des sols sableux. Le modèle offre la possibilité de représenter pré*cis*ément l'infinité de familles de courbes de compression pour des contraintes inférieures à la fractures des particules, avec un ensemble unique de paramètres. Les paramètres sont déjà estimés en partant de deux essais hydrostatiques à différentes densités dans des conditions de chargement et de déchargement. Les équations résultantes peuvent prédire l'effet de l'accroissement progressif de la rigidité et la réduction de la compressibilité alors que l'indice des vides décroît, tant pour les conditions de chargement que de déchargement. La même échelle de contrainte normalisée utilisée pour les courbes hydrostatiques peut aussi être utilisée pour décrire la ligne d'état permanent, conduisant à un schème de référence unique pour représenter les courbes contraintes–indices des vides des sols sableux. On a réalisé une série complète de simulations sur treize différents types de sols sableux, dans des conditions lâche et dense, sous une large plage de contraintes moyennes durant les conditions de chargement et déchargement. Les simulations ont donné une concordance très satisfaisante avec les résultats expérimentaux publiés.

Mots-clés : compression hydrostatique, relations constitutives, courbes contrainte–indice des vides, sols sableux.

[Traduit par la Rédaction]

Introduction

In the last 40 years, several theories and models have been developed to reproduce the observed behaviour of sandy soils. The complex nonlinear behaviour of these soils is governed by the interaction between shear and volumetric deformation, which is affected by initial packing state and stress conditions. Two main alterations to the original framework of critical state soil mechanics (Roscoe et al. 1958; Schofield and Wroth 1968) have been introduced, to better predict the combined effect of density and stress with a unique set of model parameters (Papadimitriou et al. 1999). These alterations are: (*i*) an allowance for an infinite number of hydrostatic compression curves before particle breakage becomes prevalent (as opposed to the uniqueness of this line for clays); and (*ii*) an association of the stress-dilatancy behaviour of soils with state variables defined with respect to the steady state line, such as the state parameter ψ (Been and Jefferies 1985), the state index I_s (Verdugo 1992; Ishihara 1993), and the relative void ratio r_e (Bauer 1996), among others. The implication is that the representation of the hydrostatic compression curves and steady state line plays a relevant role in constitutive modelling, especially for double-hardening models (Lade 1977; Prevost 1985; Banerjee et al. 1992), where the mechanisms of shear and volume are considered separately.

Figure 1 illustrates experimental families of hydrostatic compression curves in the void ratio – mean stress plane for a wide range of sandy soils. In general, the compression curves are nonlinear for this range of stresses, and are strongly influenced by the elastic properties of individual soil particles and by initial packing conditions in terms of soil density, fabric, and structure. The behaviour of sandy soils in this range of stresses corresponds to a true behaviour of an assemblage of particles, and plays a fundamental role in constitutive modelling (Jefferies and Been 2000). At high stress levels, it is possible to define a unique compression line associated with particle breakage, as proposed by Coop and Lee (1993) and Pestana and Whittle (1995). In principle, the stress level at which particle breakage starts and the unique compression line is reached depends not only on the

Received 21 April 2007. Accepted 7 April 2008. Published on the NRC Research Press Web site at cgj.nrc.ca on 1 August 2008.

J. Vallejos.[1] University of Chile, Department of Mining Engineering, Santiago, Chile.

[1]Present address: Queen's University, Department of Mining Engineering, Kingston, ON, Canada (email: javier.vallejos@mine.queensu.ca).

 doi:10.1139/T08-048

Fig. 1. Experimental hydrostatic compression curves for different types of sandy soils.

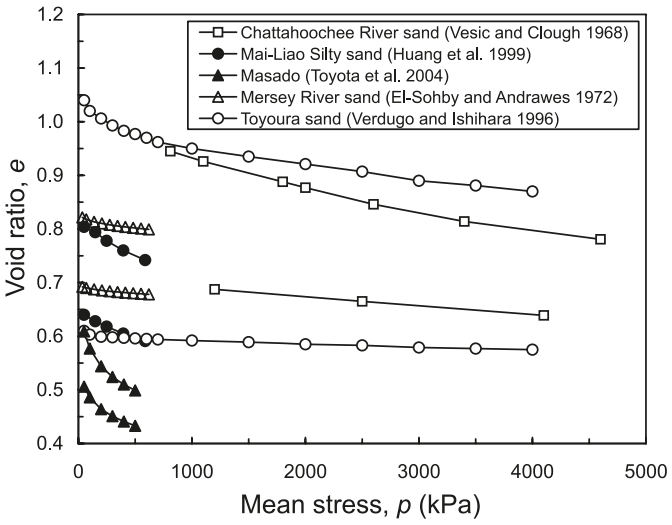

strength of the soil particles, but also on the initial density of the soil (Coop and Lee 1993).

Described in this paper is a new model for representing the infinite family of hydrostatic compression curves of sandy soils before particle crushing becomes prevalent. This model is based on the well established empirical relation of the elastic shear modulus proposed by Hardin and Richart (1963). It is also shown herein that the steady state line can be represented in the same normalized stress scale of the hydrostatic compression curves, leading to a unique framework for describing the stress–void ratio curves of sandy soils. Note that in this model, all stresses are effective and compression is assumed to be positive.

Hydrostatic compression model

A literature review (Table 1) indicates that the total volumetric deformation, ε_v, that occurs during hydrostatic loading before particle breakage becomes prevalent can be approximately described by a function of initial density packing and normalized stress, as described in eq. [1]. Proposed variations of this function are summarized in Table 1.

$$[1] \qquad \varepsilon_v = f(C_i, e_o, \alpha, p/p_r)$$

where f is a dimensionless function, C_i represents "i" dimensionless model parameters that depend on the type of material, e_o is the void ratio when $p/p_r = 0$, α is a parameter that describes the influence of the normalized stress (p/p_r), p is the mean stress (i.e., $p = (\sigma_1 + \sigma_2 + \sigma_3)/3$), and p_r is a normalizing reference stress. Three main types of models were identified. The first type corresponds to models where the influence of the void ratio and normalized mean stress are calculated using two separate and independent functions (e.g., Hansen 1967; Bauer 1996; Park and Byrne 2004). The second model type makes use of a combined function of void ratio and normalized mean stress (e.g., Hardin 1987; Pestana and Whittle 1995). In the third type of models, parameters are calibrated for each formation density (Qubain et al. 2003). Except for the Pestana and Whittle (1995) model, which is a simplified version of an original elasto-plastic model, all of the above models consider the density effect an approximation of the mean behaviour of individual tests.

The proposed model belongs to the first group of models, where the influence of the void ratio and normalized mean stress can be considered by two separate and independent functions, i.e.

$$[2] \qquad \varepsilon_v = f_1(C, e_o) f_2\left(\alpha, \frac{p}{p_r}\right)$$

where f_1 and f_2 are dimensionless functions, C and α are dimensionless model parameters, and p_r is the atmospheric pressure (~ 100 kPa). The general forms of the functions f_1 and f_2 are derived assuming an isotropic and elastic material. This assumption relates in a proportional manner to the elastic bulk modulus K ($K = dp/d\varepsilon_v$), and the elastic shear modulus G through the Poisson's ratio (i.e., $K = G[2(1+\mu)]/[3(1-2\mu)]$). Most empirical expressions for modelling the isotropic elastic shear modulus are expressed as in eq. [3] (e.g., Hardin and Richart 1963; Seed and Idriss 1970)

$$[3] \qquad G = A\ F(e)\left(\frac{p}{p_r}\right)^n$$

where A is a material constant at very small amplitudes of shear strains (approximately 10^{-6}), and $F(e)$ is a function that reflects the influence of the void ratio. In eq. [3], the elastic shear modulus is proportional to the exponential normalized mean stress $(p/p_r)^n$, where n is a model parameter that ranges between 0 and 1. This is in agreement with particle mechanics considerations (Hertz 1881; Mindlin and Deresiewicz 1953; Chang et al. 1992) and the generalized constrained modulus proposed by Janbu (1963). Equations [2] and [3] suggest that the functions f_1 and f_2 can be approximated by

$$[4a] \qquad f_1(C, e_o) \sim \frac{p_r}{A_s} \frac{1}{F(e_o)}$$

$$[4b] \qquad f_2\left(\alpha, \frac{p}{p_r}\right) \sim \frac{1}{\alpha}\left(\frac{p}{p_r}\right)^\alpha$$

where $\alpha = 1 - n$ and $A_s \sim A[2(1+\mu)]/[3(1-2\mu)]$ are two alternative model parameters. The void ratio function $F(e)$ in eq. [4a] was set at the void at zero mean stress (e_o), and treated as a constant for the purpose of integration. In eq. [4b], the function f_2 has been integrated for the case $n \neq 1$ from $p = 0$. Note that integrating f_2 with $n = 1$ will lead to the familiar straight line in the semilogarithmic plane. To simplify the analysis, the Poisson's ratio was assumed to be constant, independent of density or stress. As will be shown later, the model parameter A_s is determined directly from the experimental data, and hence it is not necessary to specify a value for the Poisson's ratio. By substituting eq. [4] in eq. [2], and assuming material particles to be incompressible (i.e., $d\varepsilon_v = -de/(1+e_o)$), the hydrostatic compression curves must appear linear in the $e - (p/p_r)^\alpha/\alpha$ plane, as shown in Fig. 2 for the Toyoura sand. As expected, the slope, $\lambda(e_o)$, decreases progressively as the void ratio decreases, indicating a reduction of compressibility.

Table 1. Hydrostatic compression models for sandy soils.

Proposed formulae used to predict volumetric deformation during hydrostatic loading before particle breakage becomes prevalent, ε_v	Comments	Reference
$C_1\ e_o^{C_2}(p/p_r)^{\alpha}$	p_r: atmospheric pressure	Hansen (1967)
$\frac{e_o}{1+e_o}\ \left\{1-\exp\left[-\left(\frac{p}{p_r}\right)^{\alpha}\right]\right\}$	p_r: granular hardness. Depends on the type of material and stress level of interest	Bauer (1996)
$\frac{1.5-D_{ro}}{C_1\ \alpha}\ (p/p_r)^{\alpha}$	p_r: atmospheric pressure α = 1/2 D_{ro}: relative density at p/p_r = 0	Park and Byrne (2004)
$\frac{e_o^2}{1+\ e_o}\ \left[\frac{(p/p_r)^{\alpha}}{C_1+\ e_o(p/p_r)^{\alpha}}\right]$	p_r: atmospheric pressure α = 1/2	Hardin (1987)
$\frac{e_o}{1+\ e_o}\ \{1-\exp[-\ C_1\ e_o^{C_2}(p/p_r)]\exp[-\ C_3(p/p_r)^{\alpha}]\}$	p_r: atmospheric pressure α = 2/3	Pestana and Whittle (1995)
$\frac{C_1\ (p/p_r)}{1+C_2\ (p/p_r)}$	p_r: atmospheric pressure C_1, C_2: calibrated for each formation density and stress level of interest	Qubain et al. (2003)

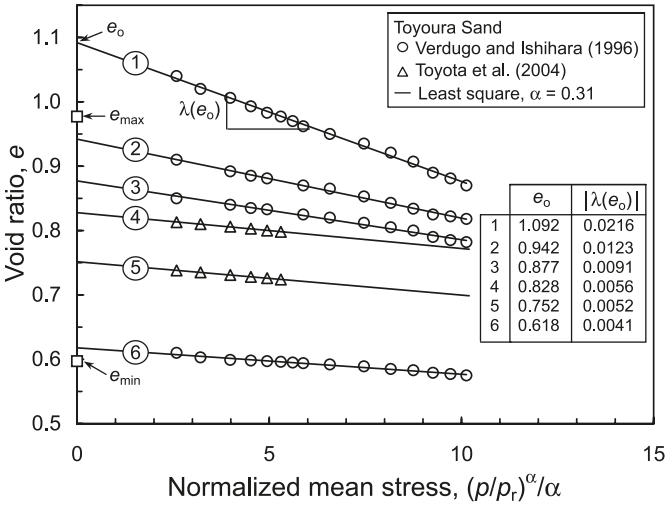

Fig. 2. Hydrostatic compression curves in the $e - (p/p_r)^{\alpha}/\alpha$ plane for the Toyoura sand.

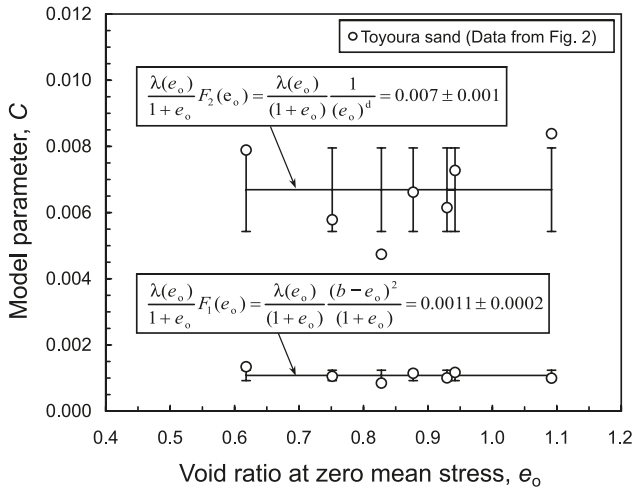

Fig. 3. Candidate functions employed to describe the effect of the void ratio on the compression curves.

The analytical form of $F(e_o)$ is determined by considering as candidates two functions that can generally be used to describe the effect of void ratio on the elastic shear modulus, namely $F_1(e_o) = (b - e_o)^2/(1 + e_o)$ (Hardin and Richart 1963; Iwasaki and Tatsuoka 1977), and $F_2(e_o) = 1/(e_o)^d$ (Hertz 1881; Biarez and Hicher 1994; Lo Presti et al. 1997), where b and d are model parameters. The most appropriate void ratio function $F(e_o)$ must satisfy eq. [5].

$$[5] \qquad \frac{\lambda(e_o)}{(1+e_o)}F(e_o) = \frac{p_r}{A_s} = C$$

Figure 3 illustrates the result of the aforementioned condition for the Toyoura sand using the two candidate functions and the adjusted values of $\lambda(e_o)$ and e_o from Fig. 2. The parameters of each void ratio function, b and d, were optimized to best fit the available data. From an examination of Fig. 3, and an observation of similar results obtained for other sands using the same condition, the void ratio function proposed by Hardin and Richart (1963) was selected. The following final model for the hydrostatic compression of sandy soils is obtained, as shown in eq. [6].

$$[6a] \qquad e = e_o - \lambda(e_o)\frac{1}{\alpha}\left(\frac{p}{p_r}\right)^{\alpha}$$

$$[6b] \qquad \lambda(e_o) = \frac{p_r}{A_s}\left(\frac{1+e_o}{b-e_o}\right)^2$$

It should be noted that the elastic shear modulus was used

as a guide to establish the general form of the functions f_1 and f_2 of the model. Therefore, the resulting alternative model parameters, A_s and b, should not be employed for the estimation of the elastic shear modulus.

Unloading–reloading

To keep the model simple and the number of parameters to a minimum, the proposed model assumes that the same relationship used for loading (eq. [6]) holds up during unloading–reloading

$$[7] \qquad e = e_{rev} + \frac{p_r}{A_s^{u-r}} \left(\frac{1+e_o^{u-r}}{b-e_o^{u-r}}\right)^2 \frac{1}{\alpha}\left[\left(\frac{p_{rev}}{p_r}\right)^{\alpha} - \left(\frac{p}{p_r}\right)^{\alpha}\right]$$

where e_{rev} and p_{rev} are the void ratio and mean stress, respectively, at the reversal point, and e_o^{u-r} is the void ratio at $p/p_r = 0$ during unloading. The additional model parameter A_s^{u-r} has dimensions of stress and can be interpreted as a stiffness property during unloading–reloading. It is implicit in eq. [7] that the model is not suitable for simulating the accumulation of plastic deformations during unloading–reloading cycles or hysteresis effects. Static problems, however, rarely involve more than one reversal point.

Model parameters and calibration

The proposed model has three input parameters that describe the hydrostatic loading behaviour of sandy soils, namely α, A_s, and b, which can be separated into two groups. The first group, comprised of α, is the usual power law used to represent the nonlinear dependency of sandy soils on mean stresses; it is assumed to be independent of density. The second group of parameters, A_s and b, control the influence of the initial void ratio on the sand behaviour. The parameter A_s has dimensions of stress, and can be interpreted as the stiffness property during loading. To calibrate the model parameters, two hydrostatic compression tests at different densities are employed as upper e_U and lower e_L reference curves. Once the parameters are determined, the hydrostatic compression behaviour can be simulated for any e–p state between these two reference curves. Ideally, the upper reference curve should be defined using the experimental hydrostatic compression curve for the loosest possible state that a given sandy soil can achieve within a given fabric. In a similar way, the lower reference curve should be defined by use of the hydrostatic compression curve for the densest state. For the common range of pressures anticipated in engineering practice, the hydrostatic compression curve for the densest state provides the lowest limit of states in the $e - p$ plane (Verdugo and Ishihara 1996). It is important to note that the hydrostatic compression curve for the loosest state depends on sample preparation method and (or) mode of deposition of the soil, while for the densest state, the hydrostatic compression curve is almost unique (Ishihara 1993).

To evaluate the parameter α and the maximum applicable stress, p_{max}, of eq. [6], a least square analysis can be performed simultaneously on the upper and lower reference curves in the $e - (p/p_r)^{\alpha}/\alpha$ plane. The selection of the parameter α is influenced by the stress level under consideration, and, as indicated by Pestana and Whittle (1995), no single power law function can fit the experimental data over the entire range of stresses. Based on this constraint, a default value of 0.5 can be used for α, which agrees with literature values (Janbu 1963; Cornforth 1974; Hardin 1987; Park and Byrne 2004), unless the available data indicates that a different value would be more appropriate. Once the value of α is determined, the adjusted values of e_{oU}, λ_U, e_{oL}, and λ_L are obtained directly from the least square fit. By application of eq. [6] to the upper and lower reference curves, eq. [8] is obtained.

$$[8] \qquad \frac{e_{oU} - e_U}{e_{oL} - e_L} = \frac{\lambda_U}{\lambda_L} = \left(\frac{1+e_{oU}}{1+e_{oL}}\right)^2 \left(\frac{b-e_{oL}}{b-e_{oU}}\right)^2$$

Equation [8] has two solutions for b, $e_{oU} < b < e_{oL}$ and $e_{oL} < b < e_{oU}$. By replacing each of these solution in eq. [6*b*], it can be demonstrated that only the first solution is feasible. This analysis enables us to obtain the following analytical expression, eq. [9], for b.

$$[9] \qquad b = \frac{\sqrt{\lambda_U}\, e_{oU}\, (1+e_{oL}) - \sqrt{\lambda_L}\, e_{oL}\, (1+e_{oU})}{\sqrt{\lambda_U}\, (1+e_{oL}) - \sqrt{\lambda_L}\, (1+e_{oU})}$$

From eq. [9], the lower limit for b is given by $b = -1$, when $\lambda_U = \lambda_L$, i.e., for an infinite family of parallel curves in the $e - (p/p_r)^{\alpha}/\alpha$ plane. Figure 4 clarifies the influence of b on the calculated compression curves for a given value of A_s. Figure 4 provides the following observations:

(1) The parameter b controls the transition of the slopes of the calculated compression curves, between the upper and lower reference curves.

(2) In terms of the compressibility of sandy soil, $b/e_{oU} > 1$ indicates compressibility decreases progressively as void ratio decreases, whereas $b/e_{oU} < 1$ indicates compressibility tends to increase as void ratio decreases.

(3) For the case $b/e_{oU} < 1$ and a fixed e_{oU}, a higher value of b decreases the influence of the void ratio on the calculated slopes of the compression curves. The opposite holds for $b/e_{oU} < 1$.

The parameter A_s is determined by substituting eq. [9] in eq. [6*b*] for any of the reference curves, to yield eq. [10].

$$[10] \qquad \frac{A_s}{p_r} = \frac{1}{\lambda_L \lambda_U}\left[\frac{\sqrt{\lambda_U}\, (1+e_{oL}) - \sqrt{\lambda_L}\, (1+e_{oU})}{e_{oU} - e_{oL}}\right]^2$$

It should be noted that, whereas the knowledge of b is necessary for the determination of A_s, b unifies the effect of the void ratio while A_s/p_r is the resulting slope in the normalized $(p/p_r)^{\alpha}/\alpha - (e_o - e)[(b-e_o)/(1+e_o)]^2$ plane, as shown in Fig. 5 for all the Erksak and the Toyoura data.

The additional unloading–reloading stiffness parameter A_s^{u-r} is evaluated from one isotropic compression test with unloading stage. Model performance during unloading–reloading can be refined by performing a series of unloading–reloading tests at different initial densities and different reversal stresses, as illustrated in Fig. 6 for the Erksak sand. As pure elasticity only exists during infinitesimal unloading, data may be scattered. The process above was applied to experimental data collected from experiments described in the literature, which were conducted on 16 differ-

Fig. 4. Influence of b on the calculated compression curves for: (*a*) $b > e_{oU}$; (*b*) $b < e_{oL}$.

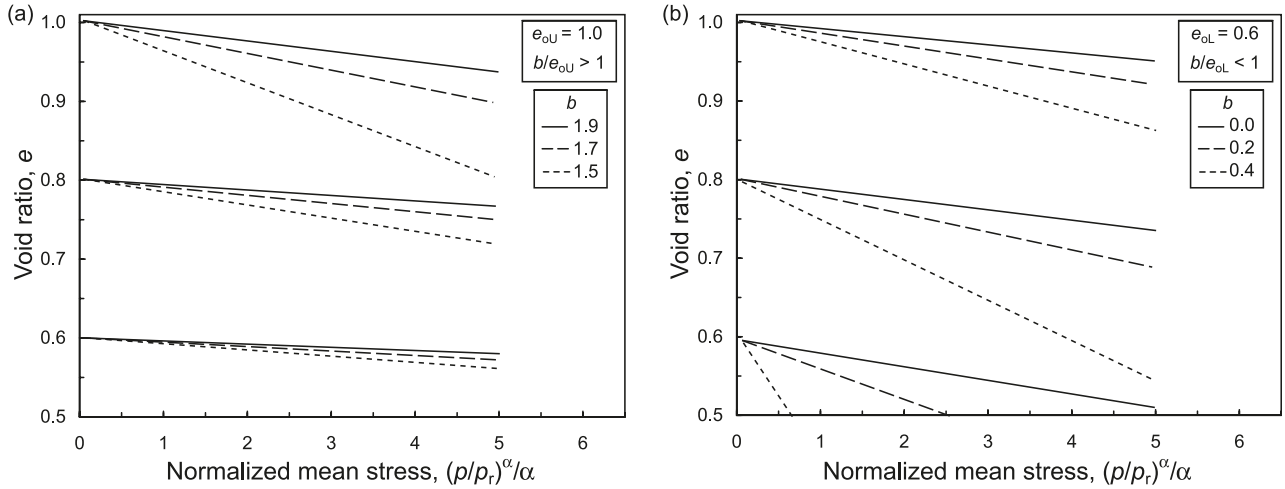

Fig. 5. Interpretation of the model parameters b and A_s for all the Toyoura and the Erksak data.

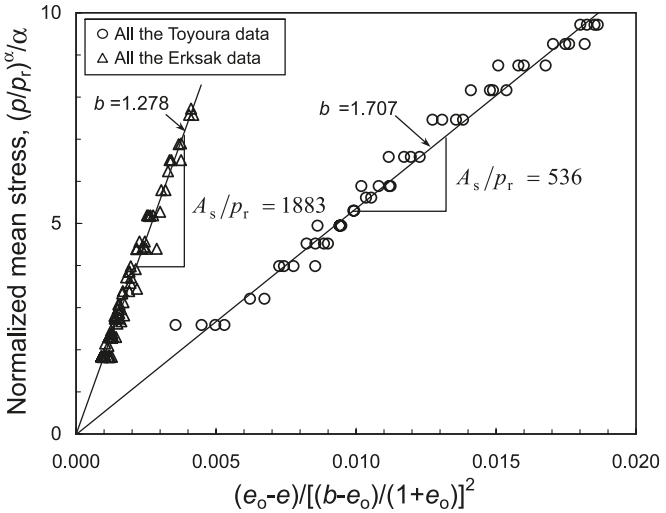

Fig. 6. Determination of the unloading–reloading stiffness parameter, A_s^{u-r}/p_r, for the Erksak sand.

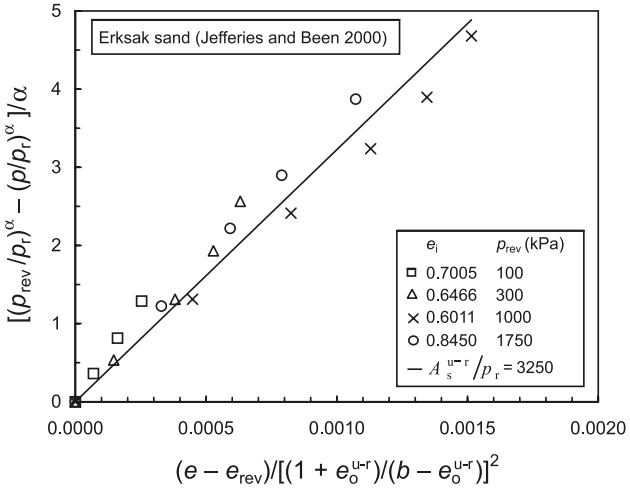

ent types of sandy soils and three granular materials. The results of the calibration procedure and the corresponding index properties for each material are presented in Table 2. When unloading conditions were not available in the experimental data set, a value equal to twice the loading stiffness was assumed. This value corresponds to the average unloading–loading stiffness ratio for clean sands (Callais, Erksak, Fuji River, Nevada, and Toyoura sands) with reported unloading stage. Examination of Table 2 provides the following preliminary findings:

(1) The proposed model's range of applicable stresses depends on the characteristics of each sandy soil. For the Toyoura sand, the applicable stress level is around 4000 kPa, while for the Chattahoochee River sand, the model gives excellent predictions for stresses between 800 and 15 000 kPa. For the carbonate Dog's Bay sand, the experimental data start to deviate from the model predictions for stresses beyond 1500 kPa. In the cases of the intact Saprolitic Tuff and Saprolitic granite, the model is able to simulate the behaviour for stress levels below 400 kPa, which corresponds approximately to a "quasi"-preconsolidation stress, as indicated by Wang and Yan (2006).

(2) The values of α can range from 0.0 to 1.0, and are influenced by the properties of the material. Generally, the values of α are lower than the 2/3 deduced from the Hertz's contact theory for the elastic compression of spherical particles. This can be partly attributed to the high rate of contact area increase, which occurs even for spherical particles, such as the Ballotini glass (Mohamed and El-Sohby 1969). The low value of α determined for the Masado indicates that a representation in the conventional $e - \ln(p/p_r)$ plane was more appropriate for this soil. The relation of the exponent of the compression modulus, $n = 1 - \alpha$, with granulometric properties has been studied before by Herle and Gudehus (1999). They concluded that, for seven sands, n decreases with decreasing C_u, increasing angularity, and increasing D_{50}. In the current study, α appeared to be qualitatively correlated with the reported particle classification for each sandy soil (see Table 2), as shown in Fig. 7. Therefore, particle shape emerges as a significant soil index property (Cho et al. 2006). It can be seen from Fig. 7 that, in general, α increases with increasing angularity. This

Table 2. Calibrated model parameters for different types of sandy soils published in the literature.

	Physical properties						Upper and lower reference curves			
Sandy soil type	e_{max}	e_{min}	D_{50} (mm)	C_u	G_s	Angularity	p_{min} (kPa)	p_{max} (kPa)	α	e_{oU}
Aio	0.958	0.582	0.40	2.7	2.63	SA-A	20	8000	0.53	0.767
Calais	0.792	0.585	0.25	1.9	2.65	SR-SA	35	650	0.36	0.785
Chattahoochee River	1.100	0.610	0.37	2.5	2.66	SA	800	14500	0.36	1.127
Dog's Bay	1.830	0.980	0.20	2.4	2.75	A	300	1500	0.99	1.782
Erksak	0.963[a]	0.521	0.33	1.8	2.65[a]	SR[a]	20	1700	0.32	0.864
Fuji River	1.030	0.480	0.40	2.1	2.73	SR-SA	20	650	0.34	0.992
Glass Ballotini 1	0.686	0.563	0.10	—	2.95	WR	30	650	0.31	0.696
Glass Ballotini 2	0.692	0.592	0.20	—	2.99	WR	30	650	0.25	0.705
Glass Ballotini 3	0.695	0.580	0.30	—	2.90	WR	30	650	0.28	0.706
Ham River	0.920	0.590	0.28	1.6	2.66	SR	50	2800	0.26	0.767
Leighton Buzzard	0.786	0.570	0.80	1.32	2.65	SR	30	650	0.24	0.808
Mersey River	0.805	0.600	0.18	1.8	2.65	SA	30	650	0.33	0.835
Nevada AP	0.857	0.573	0.18	2.3	2.65	SR-SA	40	1850	0.37	0.788
Nevada FT	0.857	0.573	0.18	2.3	2.65	SR-SA	40	1850	0.36	0.789
Sacramento River	1.030	0.610	0.21	1.5	2.68	SA	50	6000	0.87	0.870
Toyoura	0.977	0.597	0.17	1.7	2.65	SR-SA	50	4000	0.31	1.092
Mai-Liao	1.040	0.570	0.10	2.5	2.69	SA-A[c]	50	600	0.79	0.816
Masado	1.027	0.551	0.55	43.3	2.65	—	50	500	0.06	1.363
Saprolitic Granite	—	—	0.01	50.0	2.63	—	20	400	0.92	0.828
Saprolitic Tuff	—	—	0.02	4.0	2.61	—	20	350	0.54	0.844

Note: AP, air pluviation; FT, funnel deposition and tapping. A, angular; SA, subangular; SR, subrounded; WR, well rounded.

[a]From Been et al. (1987).
[b]Assumed value equal to twice the loading stiffness A_s.
[c]Grain shapes of particles retained on a No. 200 sieve.

Fig. 7. Qualitative correlation between the model parameter α and the descriptive angularity of the particles.

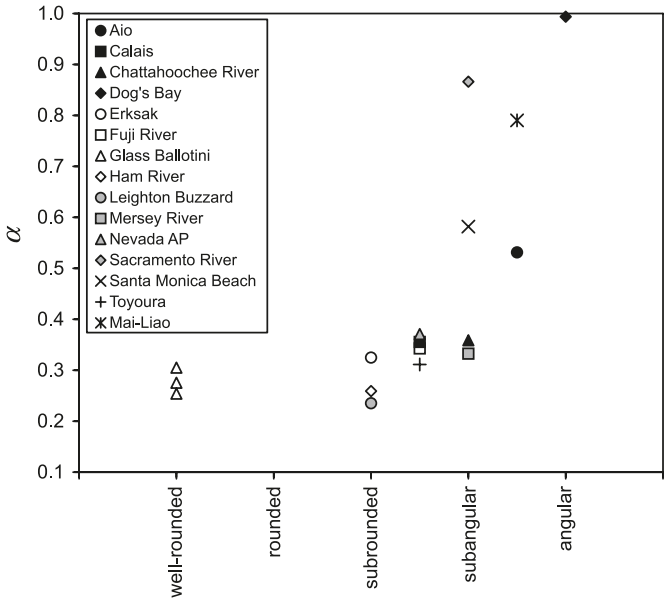

is in agreement with the previously published results of Herle and Gudehus (1999).

(3) The parameter b shows an unexpectedly narrow range for pure sand materials, between 1.2 and 1.7, with an average of 1.5 ± 0.2. There are only two noticeable outliers, the Dog's Bay sand (b = 2.454) and the Chattahoochee River sand (b = 3.831). The first could be owing to the incompleteness of data collected for the densest states of Dog's Bay sand, and the second could be attributed to the high range of stresses used to calibrate the model. The higher values of b determined for the glass and impure sandy soils reflect the low influence of the initial void ratio on the range of compression curve slopes for these types of materials. Only one case with $b/e_o < 1$ was found, and it corresponds to the Saprolitic Tuff. In this special case, the compressibility increases as the void ratio decreases. This particular behaviour was observed systematically for six of the nine experimental hydrostatic compression curves available for this soil type. This result cannot be generalized for residual soils, as the Saprolitic Granite and Masado present the expected behaviour (i.e., $b/e_o < 1$). It may just reflect the influences of formation history and (or) sampling effects, since the initial in situ void ratio of these undisturbed samples varies significantly, considering these specimens were taken from the same sampling site (Wang and Yan 2006).

(4) The parameter A_s shows a wider range of values than b, although, as mentioned previously, both parameters are correlated, as shown in Fig. 8. This correlation provides a way to estimate the parameters A_s and b with only one compression test.

Model predictions

Loading

The proposed model enables estimation of compression curves during loading and unloading conditions for any given

λ_U	e_{oL}	λ_L	b	A_s/p_r	A_s^{u-r}/p_r	A_s^{u-r}/A_s	Reference
0.0122	0.655	0.0068	1.212 ± 0.023	1291 ± 121	2612[b]± 246	2.0	Hyodo et al. (2002)
0.0054	0.606	0.0028	1.509 ± 0.011	1127 ± 32	1560 ± 55	1.4	El-Sohby and Andrawes (1972)
0.0310	0.826	0.0185	3.831 ± 0.821	20 ± 12	40[b]± 24	2.0	Vesic and Clough (1968)
0.0118	1.442	0.0040	2.454 ± 0.064	1449 ± 245	2898[b]± 491	2.0	Jovicic and Coop (1997)
0.0108	0.608	0.0031	1.278 ± 0.025	1883 ± 221	3250 ± 48	1.7	Jefferies and Been (2000)
0.0286	0.528	0.0062	1.704 ± 0.020	274 ± 15	594 ± 62	2.2	Tatsuoka (1973)
0.0040	0.570	0.0031	3.147 ± 0.265	121 ± 25	241[b]± 51	2.0	El-Sohby and Andrawes (1972)
0.0043	0.602	0.0032	1.861 ± 0.122	500 ± 102	450[b]± 205	2.0	El-Sohby and Andrawes (1972)
0.0040	0.589	0.0032	2.978 ± 0.335	139 ± 40	166[b]± 80	2.0	El-Sohby and Andrawes (1972)
0.0079	0.629	0.0038	1.197 ± 0.029	2144 ± 286	4288[b]± 571	2.0	Jovicic and Coop (1997)
0.0067	0.581	0.0032	1.669 ± 0.035	654 ± 52	1308[b]± 104	2.0	El-Sohby and Andrawes (1972)
0.0065	0.632	0.0036	1.861 ± 0.023	492 ± 21	458[b]± 46	2.0	El-Sohby and Andrawes (1972)
0.0082	0.610	0.0044	1.571 ± 0.016	637 ± 24	1577 ± 64	2.5	Lade and Abelev (2005)
0.0086	0.610	0.0043	1.458 ± 0.011	835 ± 27	1741 ± 63	2.1	Lade and Abelev (2005)
0.0034	0.608	0.0013	1.555 ± 0.022	2184 ± 132	4910[b]± 263	2.0	Lee and Seed (1967)
0.0216	0.618	0.0041	1.707 ± 0.031	536 ± 50	100 ± 24	1.9	Verdugo and Ishihara (1996)
0.0145	0.647	0.0111	5.350 ± 3.050	11 ± 14	43 ± 57	3.9	Huang et al. (1999)
0.0465	1.006	0.0308	9.647 ± 1.047	1.7 ± 0.4	5 ± 1	3.0	Toyota et al. (2004)
0.0255	0.689	0.0214	14.58 ± 2.882	0.7 ± 0.3	4 ± 1	5.2	Wang and Yan (2006)
0.0135	0.788	0.0166	0.388 ± 0.006	1209 ± 37	3765 ± 96	3.1	Wang and Yan (2006)

Fig. 8. Empirical correlation between the model parameters A_s/p_r and b for all sandy soils.

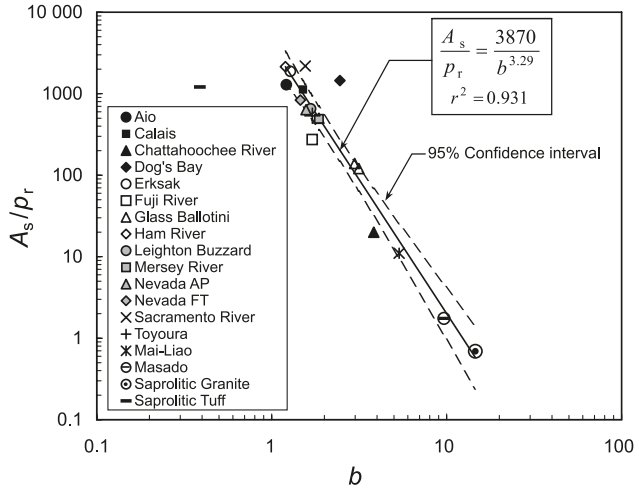

Fig. 9. Calculated compression curves from different initial void ratio – mean stress states for the Toyoura sand.

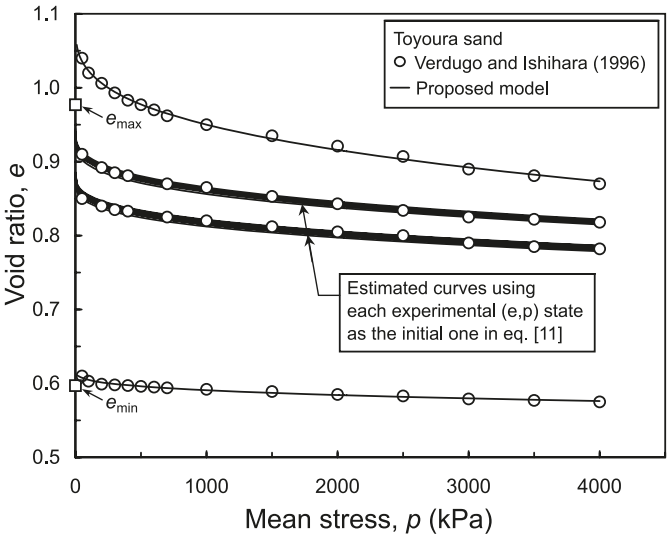

void ratio at zero mean stress between the two reference curves. The void ratio at zero mean stress can, however, only be measured and controlled in the laboratory and so for practical applications only the initial void ratio – mean stress state (e_i, p_i) is known or estimated (e.g., after consolidation or deposition). In these cases, the void ratio at zero mean stress is estimated by solving numerically the following equation.

$$[11] \qquad g(e_o) = e_o - \frac{p_r}{A_s}\left(\frac{1+e_o}{b-e_o}\right)^2 \frac{1}{\alpha}\left(\frac{p_i}{p_r}\right)^{\alpha} - e_i = 0$$

Once e_o is estimated using eq. [11], the hydrostatic compression curve corresponding to any initial (e_i, p_i) state can be established. Figure 9 illustrates the results for the Toyoura sand using the corresponding calibrated parameters presented in Table 2. Two compression curves between the upper and lower reference curves were estimated by considering each pair (e, p) of the experimental data set as the initial one in eq. [11]. It can be seen from Fig. 9 that the model is accurate enough to reproduce almost identical compression curves for any of the given initial void ratio – mean stress states that corresponds to the same compression curve.

Table 3. Coefficient of determination between measured and predicted values.

Dog's Bay		Erksak		Fuji River		Ham River		Mersey River		Nevada AP		Sacramento River		Toyoura		Mai-Liao		Saprolitic granite[a]		Saprolitic tuff[a]	
D_{ri} (%)	r^2	D_{ri} (%)	r^2	D_{ri} (%)	r^2	D_{ri} (%)	r^2	D_{ri} (%)	r^2	D_{ri} (%)	r^2	D_{ri} (%)	r^2	D_{ri} (%)	r^2	D_{ri} (%)	r^2	D_{ri} (%)	r^2	D_{ri} (%)	r^2
11	0.994	27	0.999	15	0.999	55	1.000	–8	1.000	30	1.000	39	1.000	–17	0.997	50	0.994	0	0.994	0	0.998
16	0.968	30	0.981	44	0.974	70	0.971	0	0.997	50	0.999	60	0.996	18	0.994	60	0.990	15	0.994	43	0.918
39	0.858	35	0.996	93	0.995	92	0.995	14	0.999	70	0.999	76	0.994	33	0.935	70	0.997	40	0.995	63	0.990
47	0.982	40	0.989	—	—	—	—	55	0.962	90	1.000	100	0.997	43	0.659	85	0.998	96	0.968	94	0.987
—	—	46	0.740	—	—	—	—	88	1.000	—	—	—	—	63	0.862	—	—	100	0.983	100	0.998
—	—	63	0.994	—	—	—	—	—	—	—	—	—	—	97	0.980	—	—	—	—	—	—
—	—	72	0.987	—	—	—	—	—	—	—	—	—	—	—	—	—	—	—	—	—	—
—	—	82	0.984	—	—	—	—	—	—	—	—	—	—	—	—	—	—	—	—	—	—

Note: D_{ri}, initial relative density of the sample; r^2, coefficient of determination.

[a]For the Saprolitic soils, $e_{max} = e_{oU}$, and $e_{min} = e_{oL}$ was assumed.

Fig. 10. Comparison of measured and predicted values for the Nevada sand.

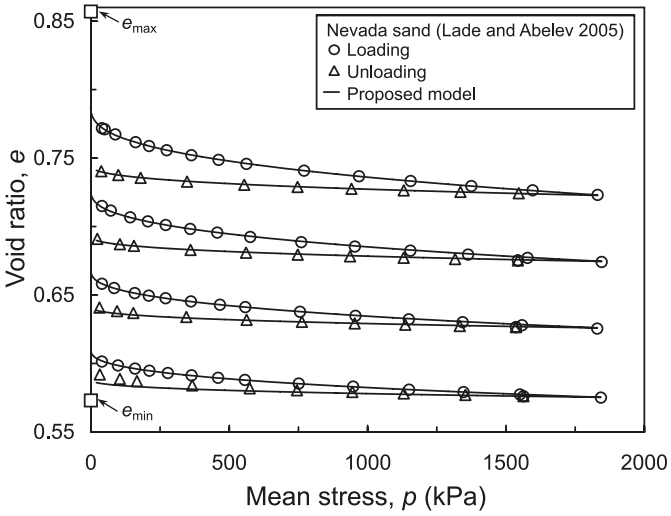

To check the performance of the developed model, Table 3 provides the coefficient of determination as an indicator of the degree of success of the predictions. In all simulations, the first (e, p) state of the experimental data set was considered as the initial one for the estimation of e_o. The proposed compression model gives highly accurate results for the eleven sandy soils presented in Table 3. Note that the simulations corresponding to Erksak, Fuji River, Mersey River, Nevada and Toyoura, span almost the entire accessible range of void ratio for these sands.

Unloading–reloading

For unloading from a reversal point (e_{rev}, p_{rev}), the void ratio e_o^{u-r} is estimated by solving an equation similar to eq. [11]. Figure 10 presents measured and predicted values for tests with one unloading stage for the Nevada sand. The model proficiently reproduces the effect of progressive increase of stiffness that occurs during loading–unloading as the initial void ratio decreases. Experimental and simulated results for tests with small and large amplitude unload–reload stages are presented in Figs. 11 and 12 for the Nevada and the Erksak sand, respectively. Expanded scales are used to improve the clarity of the comparison. Better predictions are observed for the case of the Nevada sand where the small unloading–reloading stages may induce a purely elastic response. The predictions of the model are limited for large stress reversal, which can cause some plastic straining during the unloading–reloading stage, as observed for the Erksak sand. Despite its simplicity, the model is able to reproduce the mean behaviour with satisfactory accuracy.

Steady state line

As demonstrated previously, using a unique set of parameters, the developed model is capable of accurately representing the infinite family of hydrostatic compression curves of sandy soils for a wide range of densities and stresses below particle breakage. A remarkable characteristic of the $e - (p/p_r)^\alpha/\alpha$ plane is that the steady state line can also be represented in this plane, which leads to a unique framework for describing the stress–void ratio curves of

Fig. 11. Comparison of measured and predicted values of small amplitude unload–reload stages for the Nevada sand.

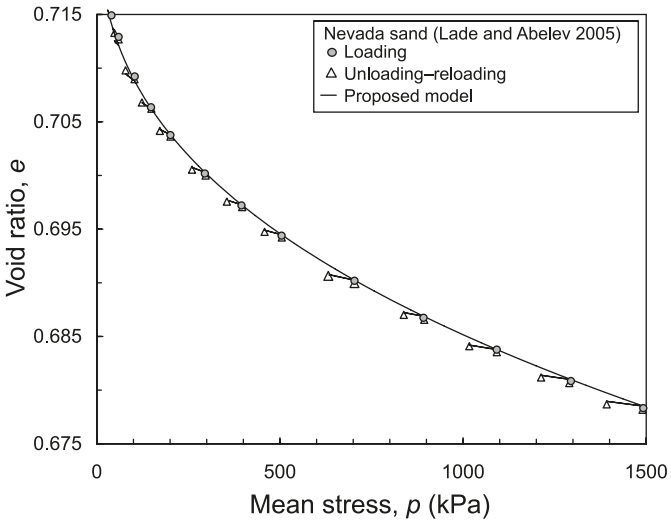

Fig. 12. Comparison of measured and predicted values of large amplitude unload–reload stages for the Erksak sand.

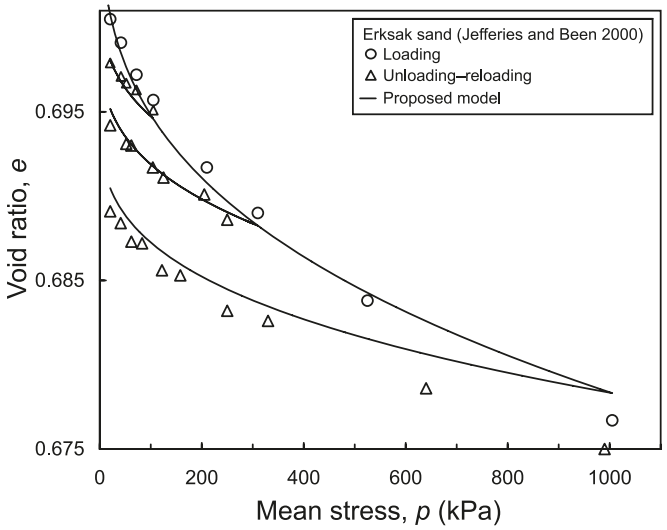

sandy soils. This normalized mean stress plane was previously proposed by Li and Wang (1998) for the linear representation of the steady state line for sands. Provided in Fig. 13 are the steady state lines for Toyoura, Erksak, and Saprolitic Tuff soils. A default value of the exponent, α_c, of 0.7 was used for both the Toyoura and Erksak sand, as proposed by Li and Wang (1998). For the case of the Saprolitic Tuff, a better representation of the steady state line was achieved with an α_c of 0.2.

Conclusions

A new four parameter model capable of accurately representing the infinite family of hydrostatic compression curves for sandy soils has been developed. Instead of approximating the effect of density to the mean behaviour of individual tests, the model is based on two well established elastic relationships that affect the behaviour of sandy soils: the proportional dependency of the modulus on the exponential

Fig. 13. Steady state lines in the $e - (p/p_r)^{\alpha}/\alpha$ plane for the Toyoura, Erksak, and Saprolitic Tuff soils.

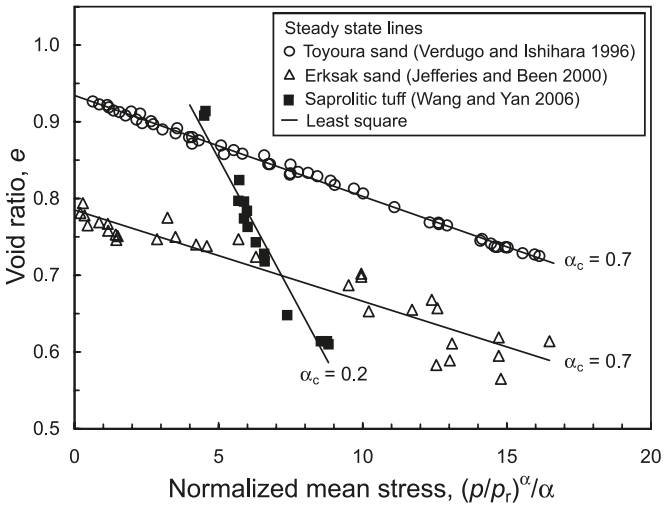

normalized mean stress, and the empirical void ratio function proposed by Hardin and Richart (1963) for the elastic shear modulus. The parameters of the model are determined directly from two hydrostatic compression tests with loading and unloading conditions set at different densities; these tests are employed as the upper and lower boundaries of the model. Once the parameters are determined, hydrostatic compression can be modelled for any void ratio – mean stress state between the two reference curves. The model can be used for stress levels encountered in most practical applications, and it is especially valuable when high stresses are not expected. The model provides a simple but accurate way of representing the hydrostatic compression curves of sandy soils in terms of total volumetric deformation. If, however, it is assumed that unloading–reloading cycles induce a purely elastic response, the total volumetric deformation can then be subdivided into elastic and plastic components. A unique conceptual framework for describing the stress–void ratio curves of sandy soils is achieved by representing the steady state line in the same normalized mean stress scale of the hydrostatic compression curves.

Acknowledgements

The author would like to thank to Dr. H. Toyota, Dr. Y.H. Wang, Dr. W.M. Yan, and Dr. P. Lade for kindly providing experimental results data. The author also thanks Ayman Tawadrous, Melissa Chappel, and two anonymous reviewers for improving the clarity and scope of the manuscript.

References

Banerjee, S., Davis, R.O., and Sribalaskandarajah, K. 1992. Simple double-hardening model for geomaterials. Journal of Geotechnical Engineering, **118**(6): 889–901. doi:10.1061/(ASCE)0733-9410(1992)118:6(889).

Bauer, E. 1996. Calibration of a comprehensive hypoplastic model for granular materials. Soils and Foundations, **36**: 13–26.

Been, K., and Jefferies, M.G. 1985. A state parameter for sands. Géotechnique, **35**(2): 99–112.

Been, K., Lingnau, B.E., Crooks, J.H.A., and Leach, B. 1987. Cone penetration test calibration for Erksak (Beaufort sea) sand. Canadian Geotechnical Journal, **24**(4): 601–610. doi:10.1139/t87-074.

Biarez, J., and Hicher, P.–Y. 1994. Elementary mechanics of soil behaviour- saturated remoulded soils. A.A. Balkema, Rotterdam.

Chang, C.S., Kabir, M.G., and Chang, Y. 1992. Micromechanics modeling for stress-strain behavior of granular soils II: Evaluation. Journal of Geotechnical Engineering, **118**(12): 1975–1992. doi:10.1061/(ASCE)0733-9410(1992)118:12(1975).

Cho, G.-C., Dodds, J., and Santamarina, J.C. 2006. Particle shape effects on packing density, stiffness, and strength: natural and crushed sands. Journal of Geotechnical and Geoenvironmental Engineering, **132**(5): 591–602. doi:10.1061/(ASCE)1090-0241(2006)132:5(591).

Coop, M.R., and Lee, I.K. 1993. The behaviour of granular soils at elevated stresses. *In* Predictive soil mechanics. *Edited by* G.T. Houlsby and A.N. Schofield. Thomas Telford, London. pp. 186–199.

Cornforth, D.H. 1974. One-dimensional consolidation curves of a medium sand. Géotechnique, **24**(4): 678–683.

El-Sohby, M.A., and Andrawes, K.Z. 1972. Deformation characteristics of granular materials under hydrostatic compression. Canadian Geotechnical Journal, **9**(4): 338–350. doi:10.1139/t72-038.

Hansen, J.B. 1967. Refined calculation of foundation movements. *In* Proceedings of the 3rd Pan-American Conference on Soils Mechanics and Foundation Engineering. Vol. III. Caracas, Venezuela. pp. 93–112.

Hardin, B.O. 1987. 1-D strain in normally consolidated cohesionless soils. Journal of Geotechnical Engineering, **113**: 1449–1467.

Hardin, B.O., and Richart, F.E. Jr. 1963. Elastic wave velocities in granular soils. Journal of the Geotechnical Engineering Division, **89**(1): 33–65.

Herle, I., and Gudehus, G. 1999. Determination of parameters of a hypoplastic constitutive model from properties of grain assemblies. Mechanics of Cohesive-frictional Materials, **4**(5): 461–486. doi:10.1002/(SICI)1099-1484(199909)4:5<461::AID-CFM71>3.0.CO;2-P.

Hertz, H. 1881. Über die beruhrung fester elasticher körper (On the contact of elastic solids). Journal Für die Reine und Angewandte Mathematick, **92**: 156–171. [In German.]

Huang, A., Hsu, H., and Chang, J. 1999. The behavior of a compressible silty fine sand. Canadian Geotechnical Journal, **36**(1): 88–101. doi:10.1139/cgj-36-1-88.

Hyodo, M., Nakata, Y., Kuwajima, K., Yoshimoto, N., and Kato, Y. 2002. Effect of fines and crushability on liquefaction of volcanic soil 'Shirasu'. *In* Proceedings of the 12th International Offshore and Polar Engineering Conference. 26–31 May 2002. Kitakyushu, Japan. pp. 529–535.

Ishihara, K. 1993. Liquefaction and flow failure during earthquakes. Géotechnique, **43**(3): 351–415.

Iwasaki, T., and Tatsuoka, F. 1977. Effect of grain size and grading on dynamic shear moduli of sands. Soils and Foundations, **17**(3): 19–35.

Janbu, N. 1963. Soil compressibility as determined by oedometer and triaxial tests. *In* Proceedings of the 3rd Danube-European Conference on Soils Mechanics and Foundation Engineering, Vol. I. Wiesbaden, Germany. pp. 19–25.

Jefferies, M., and Been, K. 2000. Implications for critical state theory from isotropic compression of sand. Géotechnique, **50**(4): 419–429.

Jovicic, V., and Coop, M.R. 1997. Stiffness of coarse grained soil at small strains. Géotechnique, **47**(3): 545–561.

Lade, P.V. 1977. Elasto-plastic stress-strain theory for cohesionless soils with curved yield surfaces. International Journal of Solids and Structures, **13**: 1019–1035. doi:10.1016/0020-7683(77)90073-7.

Lade, P.V., and Abelev, A.V. 2005. Characterization of cross-anisotropic soil deposits from isotropic compression tests. Soils and Foundations, **45**: 89–102.

Lee, K.L., and Seed, H.B. 1967. Drained strength characteristics of sands. Journal of Soils Mechanics and Foundations Division, ASCE, **93**(SM6): 117–141.

Li, X.S., and Wang, Y. 1998. Linear representation of steady-state line for sand. Journal of Geotechnical and Geoenvironmental Engineering, **124**(12): 1215–1217. doi:10.1061/(ASCE)1090-0241(1998)124:12(1215).

Lo Presti, D.C.F., Jamiolkowski, M., Pallara, O., Cavallararo, A., and Pedroni, S. 1997. Shear modulus and damping of soils. Géotechnique, **47**(3): 603–617.

Mindlin, R.D., and Deresiewicz, H. 1953. Elastic spheres in contact under varying oblique forces. Journal of Applied Mechanics, ASME, **20**(3): 327–344.

Mohamed, A., and El-Sohby, M.A. 1969. Elastic behavior of sand. Journal of Soils Mechanics and Foundations Division, ASCE, **95**(SM6): 1393–1409.

Papadimitriou, A.G., Bouckovalas, G.D., and Dafalias, Y.F. 1999. Use of elasto-plasticity to simulate cyclic sand behaviour. *In* Proceedings of the 2nd International Conference on Earthquake Geotechnical Engineering, Vol. I. Lisboa, Portugal. pp. 125–130.

Park, S., and Byrne, P.M. 2004. Stress densification and its evaluation. Canadian Geotechnical Journal, **41**(1): 181–186. doi:10.1139/t03-076.

Pestana, J.M., and Whittle, A.J. 1995. Compression model for cohesionless soils. Géotechnique, **45**(4): 611–631.

Prevost, J.H. 1985. A simple plasticity theory for frictional cohesionless soils. Soil Dynamics and Earthquake Engineering, **4**(1): 9–17. doi:10.1016/0261-7277(85)90030-0.

Qubain, B.S., Kaliakin, V.N., and Martin, J.P. 2003. Variable bulk modulus constitutive model for sand. Journal of Geotechnical and Geoenvironmental Engineering, **129**(2): 158–162. doi:10.1061/(ASCE)1090-0241(2003)129:2(158).

Roscoe, K.H., Schofield, A.N., and Wroth, C.P. 1958. On the yielding of soils. Géotechnique, **8**(1): 22–53.

Schofield, A.N., and Wroth, C.P. 1968. Critical state soil mechanics. McGraw-Hill Book Co., Inc., London.

Seed, H.B., and Idriss, I.M. 1970. Soil moduli and damping factors for dynamic response analysis. Earthquake Engineering Research Centre Report No. EERC 70–10. University of California, Berkeley, Calif.

Tatsuoka, F. 1973. Deformation mechanism of sand in triaxial compression tests: Discussion. Soils and Foundations, **13**(3): 69–73.

Toyota, H., Nakamura, K., and Kazama, M. 2004. Shear and liquefaction characteristics of sandy soils in triaxial tests. Soils and Foundations, **44**(2): 117–126.

Verdugo, R. 1992. Characterization of sandy soil behavior under large deformation. Ph.D. thesis, Department of Civil Engineering, University of Tokyo, Tokyo, Japan.

Verdugo, R., and Ishihara, K. 1996. The steady state of sandy soils. Soils and Foundations, **36**(2): 81–91.

Vesic, A.S., and Clough, G.W. 1968. Behavior of granular materials under high stresses. Journal of the Soils Mechanics and Foundations Division, ASCE, **94**(SM3): 661–688.

Wang, Y.H., and Yan, W.M. 2006. Laboratory studies of two common saprolitic soils in Hong Kong. Journal of Geotechnical and Geoenvironmental Engineering, **132**(7): 923–930. doi:10.1061/(ASCE)1090-0241(2006)132:7(923).

List of symbols

A elastic shear modulus constant

A_s loading stiffness parameter
A_s^{u-r} unloading–reloading stiffness parameter
b, d model parameters used to normalize the effect of the initial void ratio
C dimensionless model parameter related to compressibility
C_i dimensionless "i" model parameter related to compressibility
C_u coefficient of uniformity
D_{ri} initial relative density
D_{ro} relative density at $p/p_r = 0$
D_{50} particle size that is larger than 50% of the soil particles by weight
e, e_i current and initial void ratios, respectively
e_o void ratio at zero mean stress
e_o^{u-r} unloading–reloading void ratio at zero mean stress
e_{max}, e_{min} maximum and minimum void ratios
e_U, e_L upper and lower reference compression curves
e_{oU}, e_{oL} upper and lower zero mean stress void ratios
e_{rev} void ratio at reversal point
$F(e)$, $F_1(e)$, $F_2(e)$ candidate functions reflecting the influence of the void ratio on the elastic shear modulus
f, f_1, f_2 dimensionless functions
G elastic shear modulus
G_s specific gravity of particles
$g(e_o)$ equation used to estimate the void ratio at zero mean stress during loading
K elastic bulk modulus
n exponent defining the dependency of the elastic shear modulus with the normalised mean stress
p, p_r mean stress and normalising reference pressure
p_{min}, p_{max} minimum and maximum mean stress used to calibrate the model
p_{rev} mean stress at reversal point
r^2 coefficient of determination
α, α_c compression curves and steady state line exponents
ε_v total volumetric deformation
ψ state parameter
I_s state index
λ, λ_c, λ_U, λ_L hydrostatic compression, steady state, upper reference, and lower reference curve slopes in the $e - (p/p_r)^\alpha/\alpha$ plane, respectively
μ Poisson's ratio
r_e relative void ratio
σ_1, σ_2, σ_3 major, intermediate and minor principal stresses